Structural and Photocatalytic Studies with a High Activity Formate Dehydrogenase

[1,2] **Diogo Jorge Graça de Lemos Grilo**

[1] Instituto de Tecnologia Química e Biológica, Universidade Nova de Lisboa, Av. da República, 2780-157 Oeiras, Portugal
[2] Instituto Superior Técnico, Universidade de Lisboa, Av. Rovisco Pais 1, 1049-001 Lisboa, Portugal

ABSTRACT

CO_2 emissions are an urgent problem facing humanity, with an unpredictable impact on world climate. Formate dehydrogenase FdhAB from *Desulfovibrio vulgaris* is highly active for CO_2 reduction. In this work, a simplified version of FdhAB comprising only the α-subunit (FdhA) was produced. However, it showed a significant decrease in activity for formate oxidation and CO_2 reduction (5.28 and 1.34 s^{-1}, respectively for FdhA compared to 961 and 234 s^{-1}, respectively for FdhAB). Circular dichroism analysis showed a different secondary structure profile for FdhA versus FdhAB, which combined with the decrease in melting temperature (78.9 to 66.3 ºC) lead us to believe that the enzyme is unstable, highlighting the structural importance of the β-subunit. Since photocatalysis is a promising application for FdhAB, a photocatalytic setup, using the complete light spectrum, with TEOA, TiO_2 and FdhAB was successfully developed, with high formate production and turnover (5.4 mM and 42 s^{-1} after 3 h). Furthermore, TiO_2 sensitized with Eosin Y enabling visible-light absorption had also a good performance (0.6 mM of formate and 5.1 s^{-1} after 3 h). A completely metal-free setup directly coupling Eosin Y to FdhAB was also shown to work, even though with lower performance. Computational design of improved forms of FdhA and FdhAB was attempted using PROSS, with several designs obtained that need to be experimentally validated, which could help solve the stability problems of FdhA and improve even further FdhAB, that would be of high biotechnological relevance.

1. INTRODUCTION

During the next 50 years, humanity will be confronted with two major energy-related problems. On one hand, the high global demand for energy associated with the depleting fossil fuel reserves[1,2]. On the other hand, the high levels of carbon dioxide (CO_2) in the atmosphere and its effect on climate change requires an urgent and concrete response[3,4]. On this matter, carbon capture and storage (CCS) and carbon capture/utilization and storage (CCUS) technologies are getting increased attention, with the advantage of the CO_2 captured being used to generate added-value products, such as fuel[5,6]. Nonetheless, CO_2 is a highly stable molecule, making its activation a difficult process[2]. Chemical methods have proven to be inefficient and require harsh conditions[7–10], but nature has developed efficient ways of reducing CO_2, with one example being formate dehydrogenases (FDHs)[11,12], which are able to perform the two-electron reduction of CO_2 to formic acid, which is an H_2-storage material that is safe, non-flammable and non-toxic, making it highly appealing[13,14]. FDHs can be divided into metal-independent and metal-dependent enzymes. The first group mostly performs formate oxidation, with the reverse reaction happening at extremely low rates[15]. The second group is of great biotechnology relevance due to their general ability to catalyse CO_2 reduction[16–21].

Metal-dependent FDHs belong to the family of DMSO reductases, which are part of the superfamily of molybdenum/tungsten-bis pyranopterin guanosine dinucleotide-containing enzymes (Mo/W-bis PGD)[22]. FDHs are highly heterogeneous, mostly in quaternary structure and redox center composition[23,24]. Nonetheless, their active site is well-conserved, with a molybdenum or tungsten center (Mo/W) coordinated to two pyranopterin guanosine dinucleotides (PGD) forming a metal-dithiolene complex. The remaining two positions of the coordination sphere are occupied by a sulphide group (=S/-SH) and a cysteine/selenocysteine residue from the polypeptide chain[18,23–25]. Even though the active site is widely accepted, there is no consensus around the catalytic mechanism. The main issues under debate are: (i) whether the SeCys/Cys residue present in the first coordination sphere of the metal dissociates during catalysis, yielding a pentacoordinated metal[23,26–28] or if the metal remains hexacoordinated[19]. In the first case, it is proposed that the vacant position is taken by the substrate while in the second case the substrate is thought to bind the second coordination sphere; (ii) whether the reduction of the metal center occurs through the abstraction of one proton and two electrons from formate[23,24,26,27] or by a hydride transfer through the metal (directly)[28] or through the sulphide group (=S/-SH)[19,29].

Either way, several enzymes capable of efficient CO_2 reduction have been characterized, with the W/SeCys-containing FdhAB from the sulphate reducing bacteria (SRB) *Desulfovibrio vulgaris* being among the most promising[18]. FdhAB has two subunits: a catalytic (α) subunit with the active center and one [4Fe-4S] cluster and a small electron-transfer (β) subunit with three more [4Fe-4S] clusters[18].

One of the most encouraging approaches for shifting the way we utilize energy is investing in renewable green fuels, with photocatalysis gaining a center position to achieve this goal. Photocatalysis consists of using light as a source of energy to perform several types of catalytic reaction[30]. The photocatalyst, when exposed to photons with a given energy, absorb it and an electron is excited from the valency band to the conduction band[32]. A commonly used photocatalyst in studies focused on photocatalytic CO_2 reduction is titanium oxide (TiO_2), mostly due to its high abundance in nature, being non-toxic, stable, and durable[31]. The major drawback of TiO_2 is that, even though it has a high efficiency under UV irradiation, it does not respond to visible light due to its

wide bang gap, which is a limitation because only 4% of the sunlight is in the UV region, whilst 48% is in the visible region, resulting in limited efficiency[31]. Sensitization with organic dyes can be used to address this issue, since they can absorb visible light and inject the electrons in the conduction band of the semiconductor, initiating the photocatalytic cascade[30,32]. Xanthenes, such as Eosin Y (EY), are being widely used, mostly because of their low cost, good visible absorption properties, commercial availability, and being metal-free[30]. For the system to be able to be subjected to several cycles, a sacrificial electron donor (SED) is used to regenerate the photoexcited molecule[33]. However, it is not easy to rationalize and predict how a SED will behave in a system since the environment will influence its behaviour[30,33].

With this in mind, the first goal of this work was to produce a simplified version of FdhAB composed only of the catalytic subunit and characterize it. A similar study has already been carried out with success with a [Ni-Fe] hydrogenase, where the electron transfer subunit was removed and the authors were still able to obtain the catalytic subunit with full cofactor loading, nonetheless with significant decreases in activity for hydrogen-deuterium exchange (H_2 splitting capacity)[34].

The second goal of this work was to develop different photocatalytic setups for CO_2 reduction with FdhAB, which would allow us to have an efficient, commercially available system to test enzyme variants, using the already existing knowledge that FdhAB strongly interacts with TiO_2 nanoparticles[35] and that EY, a cheap commercially available dye, and TiO_2 have already been coupled successfully for hydrogen generation[36].

As a third goal and already anticipating that the removal of an entire subunit can lead to stability issues, as seen in for the [Ni-Fe] hydrogenase[34], the *in silico* stabilization of FdhA variant using PROSS[37] based on the highly popular design software Rosetta was attempted. PROSS uses as input a position-specific substitution matrix (PSSM), which represents the log-likelihood of observing any of the 20 canonical amino acids at a given position. Mutations with a score ≥ 0 are considered favourable, using the reasoning that deleterious mutations are rare or absent due to natural selection and that the most frequent amino acids at a given position may indicate stability. In a second stage, Rosetta calculations are used to obtain the energy difference between the wild-type and a given single-point mutant (ΔGG_{calc}), for all single-point mutations considered by the first step. The mutations that surpass both stages of selection are used by Rosetta combinatorial sequence design, generating a final model that needs to be experimentally validated[37]. Furthermore, due to the existence of marginal stability in natural proteins, the great majority of them have room for improvement, in terms of both stability and functionality[38]. Therefore, in parallel, an attempt to improve FdhAB stability was also pursued. Understanding how to improve FdhAB stability and its variants may bring important information that could potentiate the biotechnological use of this enzyme as a biocatalyst for CO_2 reduction.

2. MATERIALS AND METHODS

Generation of a pRec-FdhA-Strep Plasmid

The plasmid pRec-FdhAB-Strep[18] was mutated to add an *Eco*RI restriction site by site-directed mutagenesis (primers from Invitrogen and mutagenesis done using NZYMutagenesisKit protocol with *E. coli* DH5α competent cells), flanking the *KanR* cassette near the RBS of KanR, with a site downstream *fdhB* for *Eco*RI being already present in the plasmid. After transformation, cells were plated onto LB Agar (25 g/L LB Broth with 15 g/L Agar) with spectinomycin (100 µg/mL) and grown at 37 ºC overnight. Colonies were collected and grown on LB medium with spectinomycin (100 µg/mL) at 37 ºC overnight. The plasmid was extracted using the plasmid DNA Miniprep NZYTech Kit. The plasmid was digested with *Eco*RI for 37 ºC and 1 hour, followed by an inactivation step of 20 minutes at 65 ºC. The product was analysed using an agarose gel, and the band corresponding to the desired plasmid fragment (7875 bp) was extracted using GeneJET Gel Extraction Kit from Thermo Fisher. Ligation was done with T4 DNA Ligase (BioLabs Inc., New England) for 2.5 hours at room temperature, followed by an inactivation step of 10 minutes at 65 ºC. The generated pRec-FdhA-Strep was transformed into *E. coli* DH5α competent cells, being grown as stated before. A colony PCR was performed with primers flanking the region where the *fdhB* gene was situated, yielding in positive colonies a band with 3893 bp. In positive colonies, the plasmid was sent to sequence for confirmation (GATC Biotech, Germany).

Generation of a DvFdhA Mutant

A *D. vulgaris ΔfdhAB* deletion strain was grown in MOYLS medium pH 7.2 (8 mM $MgCl_2$, 20 mM NH_4Cl, 0.6 mM $CaCl_2$, 2 mM K_2HPO_4-NaH_2PO_4, 0.6% (v/v) Trace Elements (0.5 g/L $MnCl_2$•$4H_2O$, 0.3 g/L $CoCl_2$•$4H_2O$, 0.2 g/L $ZnCl_2$, 0.05 g/L Na_2MoO_4•$4H_2O$, 0.02 g/L H_3BO_3, 0.1 g/L $NiSO_4$•$6H_2O$, 0.09 g/L $NiCl_2$•$6H_2O$, 0.002 g/L $CuCl_2$•$2H_2O$, 0.006 g/L Na_2SeO_3•$5H_2O$, 0.008 g/L Na_2WO_4•$2H_2O$), 0.06 mM $FeCl_2$, 0.12 mM EDTA, 30 mM Tris-HCl 2 M, 0.1% (v/v) Thauers Vitamins 10 X, 1.2 mM Thioglycolate, 1 g/L Yeast Extract, 30 mM Lactate 1 M, 30 mM Sulphate). When OD=0.2 was reached, cells were electroporated, as described in [39] with the constructed plasmid (1250 V, 250 Ω, and 25 µF using Gene Pulse Xcell, Bio-Rad) and left anaerobically in MOYLS medium overnight at 37 ºC. Cells were plated in MOYLS with Agar (15 g/L) and spectinomycin (100 µg/mL) and grown for 6 days in anaerobiosis at 37 ºC. Selected colonies were grown in liquid MOYLS until an OD=0.6-0.8 and then cells were inoculated in Postgate Medium C (3.7 mM KH_2PO_4, 18.7 mM NH_4Cl, 17.6 mM Na_2SO_4, 0.4 mM $CaCl_2$•$2H_2O$, 0.24 mM $MgSO_4$•$7H_2O$, 0.4 g/L Yeast Extract, 26 µM $FeSO_4$•$7H_2O$, 1 mM sodium citrate tribasic dihydrate, 0.57 mM L-ascorbic acid, 0.88 mM sodium thioglycolate, 40

mM sodium formate, 10 mM sodium DL-lactate and 100 mM Tris base, supplemented with 10 µM of $NiCl_2$•$6H_2O$/Na2SeO3•$5H_2O$ and 10 µM of Na_2O_4W•$2H_2O$). After 24 h, cells were recovered and stored at -20 ºC and the plasmid extracted and sequenced, as previously done.

Protein Purification by Affinity Chromatography

D. vulgaris Hildenborough cells from a large scale-growth expressing the protein of interest were retrieved and resuspended in binding buffer (100 mM Tris-HCl pH 8.0, 150 mM NaCl, 10 mM $NaNO_3$, 10% (v/v) glycerol) and DNAse was added. The resuspended cells were disrupted in a French Press, and the crude extract was subjected to centrifugation at 8000 g for 20 minutes at 4 ºC. The supernatant was then subjected to ultracentrifugation at 109 000 g for 2 hours at 4 ºC. The resulting supernatant was recovered, and protease inhibitor was added, obtaining the soluble fraction, which was centrifuged at 48 000 g for 30 minutes at 4 ºC, being further loaded on a Strep-tactin gravity flow (IBA Lifesciences, Germany) affinity column equilibrated with binding buffer. After 5 washing steps with binding buffer, 8 elution steps were carried using elution buffer (binding buffer supplemented with 2.5 mM D-desthiobiotin), being the first 2 pooled together (Elution A) and the remaining 6 pooled together (Elution B). The fractions that were collected during the loading and washing steps (flow-through) were subjected to another round of affinity chromatography, as described. The buffer of the eluted fractions was changed to sample buffer (20 mM Tris-HCl pH 7.6, 10 mM $NaNO_3$, 10% (v/v) glycerol) and stored at 4 ºC for immediate use or at -20 ºC for longer periods. In samples purified anaerobically, all steps were performed anaerobically, and the affinity chromatography setup was done inside a COY Anaerobic Chamber (atmosphere of 2% H_2/98% N_2) at room temperature. The purity of each sample was evaluated by a 12% SDS-polyacrylamide gel.

FdhA Purification by Ion Exchange Chromatography

Samples were centrifuged at 17 000 g for 20 minutes at 4 ºC, with the supernatant being then loaded on a 6 mL Q-Resource™ column (Pharmacia Biotech), equilibrated with sample buffer. The column elution was performed at a flow rate of 1 mL/min with stepwise increments of NaCl (25-50 mM NaCl), until 200 mM NaCl, then a linear gradient was applied until a concentration of 1 M NaCl or a two-step increment with 500 mM NaCl and 1 M NaCl were performed. To evaluate the purification, a 12% SDS-polyacrylamide gel was run.

Protein Concentration

The samples obtained after purification were quantified by Nanodrop ND200C, for FdhAB the Lambert-Beer Law was used ($\varepsilon_{410\ nm}$ = 43.25 $mM^{-1}.cm^{-1}$), while for FdhA, the following rationale was used:

$$When\ Abs_{260\ nm} > Abs_{280\ nm} \rightarrow [Protein](mg/mL) = 1.55 \times Abs_{280\ nm} - 0.76 \times Abs_{260\ nm} \quad (eq.1)$$

$$When\ Abs_{260\ nm} < Abs_{280\ nm} \rightarrow [Protein](mg/mL) = Abs_{280\ nm} \quad (eq.2)$$

For the kinetic analysis of FdhA, the protein was quantified by BCA (BCA Protein Assay Kit from Novagen) or by the estimated $\varepsilon_{410\ nm}$ determined for FdhA ($\varepsilon_{410\ nm}$ = 91.13 $mM^{-1}.cm^{-1}$). For circular dichroism spectroscopy, both FdhA and FdhAB were quantified using BCA. For the thermal-shift assay, quantification of FdhA and FdhAB were estimated using their respective $\varepsilon_{410\ nm}$.

Western-blot

Cell disruption was carried using BugBuster Protein Extraction Reagent (Novagen, Inc.). The soluble fraction was then run on a 12% polyacrylamide gel and transferred using a Mini Trans-Blot Electrophoretic Transfer Cell (Bio-Rad) to a polyvinylidene difluoride membrane (PVDF membrane) during 1 h at 350 mA (150 V, 100 W) at 4 °C. The membrane was then left to dry overnight. On the next day, the membrane was blocked with PBS blocking buffer (PBS Buffer with 3% BSA, 0.5% (v/v) Tween 20) for 1 h at room temperature and mild agitation. Afterwards, three washing steps are performed (5 minutes each) with PBS Buffer with 0.1 % Tween 20. The membrane was then incubated with Biotin Blocking Buffer (IBA Lifesciences, Germany) for 10 minutes and then treated with Strep-Tactin antibody labelled with alkaline phosphatase (IBA Lifesciences, Germany) diluted 1:4000 for 1 hour at room temperature and mild agitation. Two washing steps are then performed (1 minute each) with PBS Buffer with 0.1% Tween 20. Immunodetection was performed, protected from light, in 100 mM Tris HCl pH 8.0, 100 mM NaCl and 5 mM $MgCl_2$ with nitro-blue tetrazolium and 5-bromo-4-chloro-3'-indolyphosphate (NBT-BCIP) (Sigma-Aldrich) during 2h30 at room temperature and mild agitation. The reaction was stopped with distilled water.

Activity-stained Native Gel

Soluble fractions (50 µg) purified using the BugBuster protocol for FdhA and using the French press protocol for FdhAB were run in a native polyacrylamide gel (7.5%) containing 0.1% Triton X-100 to evaluate formate oxidation activity. The gel was incubated in a solution of 50 mM Tris-HCl buffer pH 7.6, 20 mM sodium formate, 0.908 mM DTT and 0.625 mM benzyl viologen, under a N_2 atmosphere. When bands were visible, they were fixed by the addition of 10 mM of 2,3,5-triphenyltetrazolium chloride solution.

Activity Assays and Kinetic Analysis

Activity assays were performed in a COY Anaerobic Chamber (atmosphere of 2% H_2/98% N_2) at room temperature under constant stirring, using a UV-1800 Shimazu spectrophotometer. The assays for formate oxidation and CO_2 reduction activity were performed after pre-incubation of the enzyme (1.4 nM and 0.9 nM final concentration in the assays, for FdhAB and FdhA, respectively) with 50 or 500 mM DTT, for FdhAB and FdhA, respectively, for 5 minutes. For formate oxidation, the pre-incubated enzyme was added to a cuvette with 50 mM KPi pH 7.6, 1 mM DTT and 2 mM benzyl viologen. After 30 seconds the reaction was initiated by the addition

of 20 mM of formate. For CO_2 reduction, the reaction was started by adding the pre-incubated enzyme to a cuvette with 50 mM KPi pH 6.9, 1 mM DTT, Zn-reduced methyl viologen (adjusted to an absorbance of 1) and 50 mM sodium bicarbonate (final pH 7.1). Formate oxidation was followed by the reduction of benzyl viologen at 555 nm ($\varepsilon_{555\ nm}(BV^+)$ = 12 $mM^{-1}.cm^{-1}$) and CO_2 reduction by the oxidation of methyl viologen at 578 nm ($\varepsilon_{578\ nm}(MV^+)$ = 9.7 $mM^{-1}.cm^{-1}$). One enzymatic unit (U) was defined as the amount of FDH capable of oxidizing/reducing 1 µmol of formate/CO_2 per minute.

O_2 Exposure Assays

Anaerobic purified FdhA was diluted in aerobic sample buffer to a final concentration of 2.8 µM and exposed to air for 8 h at room temperature. At several timepoints, samples were collected, and activities were measured as described before.

Circular Dichroism Spectroscopy

FdhA (0.04 mg/mL) and FdhAB (0.20 mg/mL) in sample buffer without $NaNO_3$ were analysed using a 0.1 cm path length quartz cuvette in a Jasco J-815 CD spectropolarimeter from 200 nm to 250 nm with a data pitch of 0.1 nm and accumulation of 2 scans, using a scanning speed of 50 nm/min. The results were analysed using Beta Structure Selection webserver (BeStSel)[40,41].

Thermal Shift Assay

Samples recovered from the circular dichroism spectroscopy were concentrated to values of 0.05 mg/mL and 0.45 mg/mL for FdhA and FdhAB, respectively. The Applied Biosystems Protein Thermal Shift Dye kit was used to determine the melting temperatures of both proteins, the enzymes were mixed with the dye (2x-fold). The melting curve was recorded from 25 to 99 °C on the QuantStudio 7 Flex Real-time PCR System from Applied Biosystems.

Photocatalytic Assays

Photocatalytic reactions were carried out anaerobically in 11 mL flasks with a working volume of 5 mL. The buffer used was 20 mM Tris HCl pH 7. TiO_2 nanoparticles (Acros Organics) (0.4 – 2.7 mg/mL) were dispersed in the buffer. When EY was used, the dye was added after the dispersion of the nanoparticles in the solution, and a 15-minute incubation under agitation was done in the dark and, when TiO_2 was not used, it was directly added to the reaction flask. EY concentration used varied between 0.22 mM and 0.88 mM. Furthermore, 100 mM TEOA (pH 1.9) or 100 mM of a mixture of Cystein/HCl-Cystein (6:1 ratio) was added, followed by 100 mM of sodium hydrogen carbonate, as CO_2 source. The enzyme (12 nM), previously incubated with 50 mM of DTT for 5 minutes was the last component added before light exposure with LEDs (λ = 470 nm; I = 7 W/m^2) or a Solar Simulator with a 300 W Xenon Lamp (Sirius-300P, Zolix) ($I_{340\text{-}450\ nm}$ = 7000 W/m^2). The experiments using LEDs were performed inside a 4 °C room (system temperature of 25 °C), while in the Solar Simulator a water bath at 25 °C was used (system temperature of 35 °C). The flasks were under continuous stirring during the process. At several timepoints, 200 µL of each reaction were centrifuged at 17 000 g for 10 minutes at 4 ºC and frozen at – 20 °C. Formate concentration was then determined by high performance liquid chromatography (HPLC), using a Waters Alliance 2695 chromatographer (Waters Chromatography, Milford, MA) connected to a Waters 2996 Photodiode Array Detector set at 206.5 nm. Chromatography separation was undertaken using an Aminex HPX-87H column (300 x 7.8 mm), 9 µm particle size (Bio-Rad, Hercules, California) and set at 60 °C. Elution was carried out isocratically, at a flow rate of 0.5 $mL.min^{-1}$, with 0.005 M of H_2SO_4 and the volume injected was 100 µL. The formate retention time obtained was 15.9 min. Data acquisition was accomplished with the Empower 2 software (Waters Chromatography).

***In silico* Stabilization of the Enzyme**

For the computational stabilization, an unpublished x-ray structure of FdhAB was used. The full structure was used for FdhAB design and only the α-subunit for FdhA design. The stabilization of the enzyme was divided into three parts as previously done in PROSS protocol[37]: preparation of the structure, filterscan and design. In all steps, the energy function ref2015 was used with harmonic backbone coordinate restraints set to the coordinates observed in the crystal structure[42]. In the preparation, the active site was modelled as a rigid body (MGDs, W and S atoms), hydrogens were added at pH 7.2 and the structure was relaxed using Avogadro[43]. The conserved $SeCys_{192}$ was modelled as a cysteine and the structures with the presence of the active site were scored, renumbered, and relaxed (with the Rosetta relax protocol). The filterscan was performed as described in PROSS[37], with the PSSM used being generated through a MSA using PSI-BLAST[44] with refseq_selected database. The sequences were clustered using CD-HIT[45]. Mutations allowed were defined as having a PSSM score ≥ 0 and considering 8 different thresholds: ΔGG ≤ +0.5, ΔGG -0.45, ΔGG ≤ -0.75, ΔGG ≤ -1.0, ΔGG ≤ -1.25, ΔGG ≤ -1.5, ΔGG ≤ -1.8 and ΔGG ≤ -2.0 kcal/mol[37]. The design protocol was performed using Rosetta combinatorial sequence design[37]. In FdhAB, the filterscan and design steps were performed in each subunit separately, but in the presence of the whole complex. In both cases, the residues at 4 Å from the active center and from the iron-sulphur clusters were fixed and restricted, with the selection being carried using Visual Molecular Dynamics (VMD) software[46]. The analysis of each design was done using FeaturesReporter suite[47]. For the determination of the core region of the protein, residue burial was defined as in [37]. The isoelectric points were calculated using ExPASy webserver[48].

3. RESULTS

Generation, Purification and Characterization of FdhA

Since the catalytic center of FdhAB is present in the α-subunit, which also harbours an iron-sulphur cluster, it can be theorized that the large subunit of the enzyme harbours the minimal number of centers crucial for catalysis. Therefore, to generate a mutant *D. vulgaris* strain only expressing the α-subunit of FdhA, in the expression plasmid of FdhAB-Strep was introduced a second restriction site for *Eco*RI, which allowed for the removal of the sequence corresponding to FdhB. The genetic manipulation was successfully achieved and confirmed by sequence. The plasmid was then successfully transformed into a *ΔfdhAB D. vulgaris* Hildenborough, generating a mutant strain expressing the recombinant FdhA. To evaluate the expression of FdhA, a Western-blot against Strep-tag and an activity-stained native gel were performed.

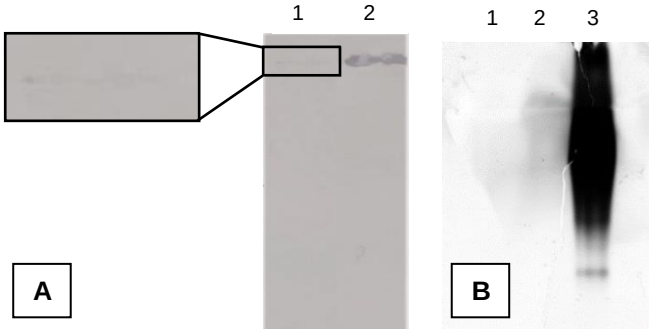

Figure 1: (A) Western-blot of the soluble extract collected from *D. vulgaris* Hildenborough strain expressing the recombinant FdhA protein (Lane 1 – 10 µg) and a strain expressing the recombinant FdhAB protein (Lane 2 - 10 µg) **(B)** Native-polyacrylamide gel (12%) revealed for formate oxidation (reduction of benzyl viologen) with a soluble extract from a strain expressing the FdhA protein (Lane 1 – 50 µg) and other expressing the FdhAB protein (Lane 3 – 50 µg).

For these reasons, although expression is obtained, it appears that the expression and/or degradation kinetics of FdhA are altered in comparison to FdhAB. Even though no activity was seen, it is not possible to conclude that FdhA is not active, since the negative result can be attributed to increased oxygen susceptibility (losing activity when exposed to air during purification) or if the activity is below the detection limit of the technique. With this in mind, a large growth was performed and to understand if oxygen was damaging the protein, both an anaerobic and aerobic purification were carried out. Furthermore, to compare the simplified version of the protein, FdhAB was also purified using the same method. For each purification, two elutions (Elution A and Elution B) were obtained and analysed by SDS-PAGE.

The FdhAB protein with the strep-tag has a molecular mass of 138.32 kDa, with the α-subunit having 108.8 kDa and the β-subunit 26.4 kDa, which is consistent with the bands observed in the lanes of the Elutions A and B (Figure 2A). Nonetheless, Elution B is purer and was the one used in the following analysis.

Regarding FdhA, in both aerobic and anaerobic purification, it is possible to observe that the protein was successfully obtained in Elution A and B (Figure 2B and Figure 2C). The profile in terms of contaminants both in Elution A and Elution B was quite similar in the sample purified aerobically and anaerobically and in both cases Elution B is purer than Elution A, nonetheless not as pure as the one obtained for FdhAB.

To understand if the simplified enzyme is less tolerant to oxygen, the anaerobically purified FdhA was subjected to oxygen at room temperature, with both formate oxidation and CO_2 reduction of the enzyme being measured to analyse the effect of oxygen over time. In

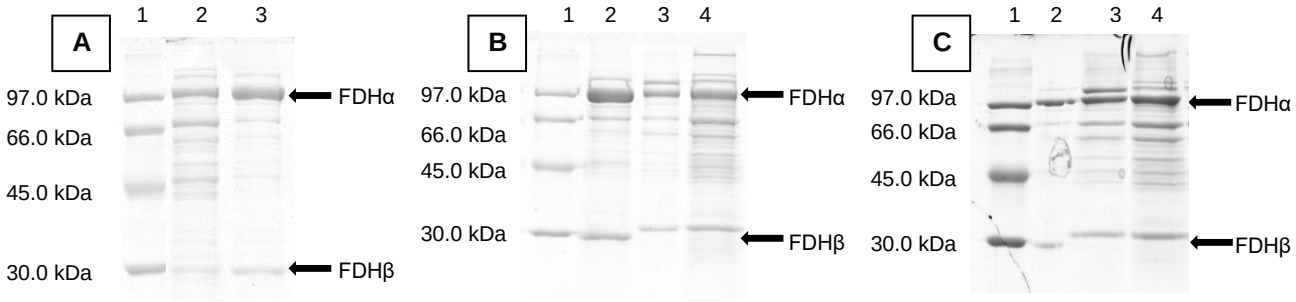

Figure 2: SDS-polyacrylamide gel (12%) to analyse the elutions obtained after aerobic purification of FdhAB **(A)**, aerobic **(B)** and anaerobic **(C)** purification of FdhA. In **(A), (B) and (C)**: Lane 1: Amersham Low Molecular Weight Calibration Kit for SDS Electrophoresis (97.0 kDa, 66.0 kDa, 45.0 kDa, 30.0 kDa). In **(A)**: Lane 2: 10 µg Elution A FdhAB purification; Lane 3: 10 µg Elution B FdhAB purification. In **(B)**: Lane 2: 10 µg Elution B FdhAB purification; Lane 3: 10 µg Elution B FdhA purified aerobically; Lane 4: 10 µg Elution A FdhA purified aerobically. In **(C)**: Lane 3: 4 µg Elution B FdhA purified anaerobically; Lane 4: 6.55 µg Elution A FdhA purified anaerobically.

In the Western-blot (Figure 1A), when zooming in the region of the molecular weight of the α-subunit (108.8 kDa), an extremely tenuous band is present (lane 1), indicating expression, even though low in comparison to FdhAB (lane 2). Furthermore, no formate oxidation activity was detected for FdhA (Figure 1B), even when increasing protein quantities (up to 200 µg – result not shown), contrasting with the high activity seen for FdhAB (lane 3).

both reaction directions, even though with some fluctuations due to low reproducibility mostly in CO_2 reduction, the enzyme appears not to be susceptible to O_2 in the timeframe studied (8 hours), allowing aerobic handling and purification, as seen for FdhAB[18].

To structurally and kinetically characterize FdhA, a second purification step of the aerobically purified FdhA was performed to obtain purer samples. Both Elutions A and B were loaded, individually, on a Q-resource™

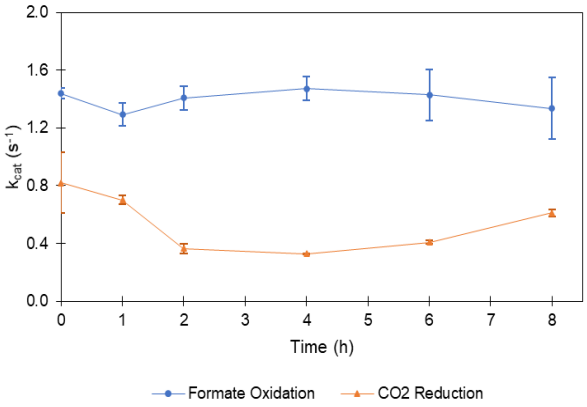

Figure 3: FdhA purified anaerobically was exposed to air with formate oxidation activity (blue circles) and CO_2 reduction activity (orange triangles) being measured at multiple timepoints. The error bars represent the standard deviation of three assays.

column, equilibrated with sample buffer. The elution was done by increasing NaCl concentration. The eluted samples were divided into several fractions, quantified, and analysed by SDS-PAGE (Figure 4A and B, for Elution A and B purification, respectively). It was possible to obtain a pure sample of FdhA in fractions 1 and 2 of Elution A, nonetheless the band had low intensity. Since the yields of proteins were low, both fractions were pooled together to minimize protein loss in quantification methods, and this sample was used in the structural analysis. In the purification of Elution B, fraction 2 appeared to be more enriched in FdhA, even though a contaminant was still present. This fraction was used for kinetic analysis.

The structural analysis was performed first by circular dichroism spectroscopy (CD), which is widely used for rapid and simple prediction of secondary structure[41]. To estimate the % of each type of secondary structure from FdhA and FdhAB using CD data, BeStSel was used (Table 1)[40,41]. Notoriously, even though the general proportion of α-helixes varied only slightly, when comparing Helix1 and Helix2 it is observable that the difference can be attributed to less regular α-helixes in the structure of FdhA (3.3%) versus FdhAB (6.0%). The presence of the β-subunit would not explain this difference since from the oxidized x-ray crystal structure of FdhAB (PDB code:6SDR) it is possible to obtain the % of each secondary structure component and FdhB has even a smaller % of α-helix versus FdhA (about 1% difference). The major difference in secondary structure was seen in antiparallel β-sheets where there is a complete absence of this type of secondary structure in FdhA, while it comprehended about 22% of secondary structure composition in the FdhAB protein. This difference was quite evident and, since there was an increase as well in about 20% in the category defined as others for FdhA, it is quite probable that most antiparallel β-sheets are disorganized in the FdhA protein. With these results, FdhA appears to have a different folding than FdhAB, however, it is not possible to analyse if the difference is seen in a particular region or if it is a global folding problem.

Table 1: Predicted secondary structure composition (%) for FdhAB and FdhA obtained using BeStSel[40,41]. The types of structures are divided in α-helixes (regular α-helixes - middle part - and distorted α-helixes - the two residues at each end of the helix -), parallel β-strands, antiparallel β-strands (left-twisted, relaxed and right-twisted), turns, and others (structures such as 3_{10}-helix, π-helix, β-bridge, bends, loop/irregular and invisible regions of the structure).

Secondary Structure Type		Secondary Structure Composition	
		FdhAB	**FdhA**
Helix-α	Helix1 (regular)	6.0%	3.3%
	Helix2 (distorted)	7.3%	7.5%
Parallel β-strands		12%	15%
Antiparallel β-strands	Anti1 (left-twisted)	5.6%	0%
	Anti2 (relaxed)	11.5%	
	Anti3 (right-twisted)	4.3%	
Turns		12%	13%
Others		41%	61%

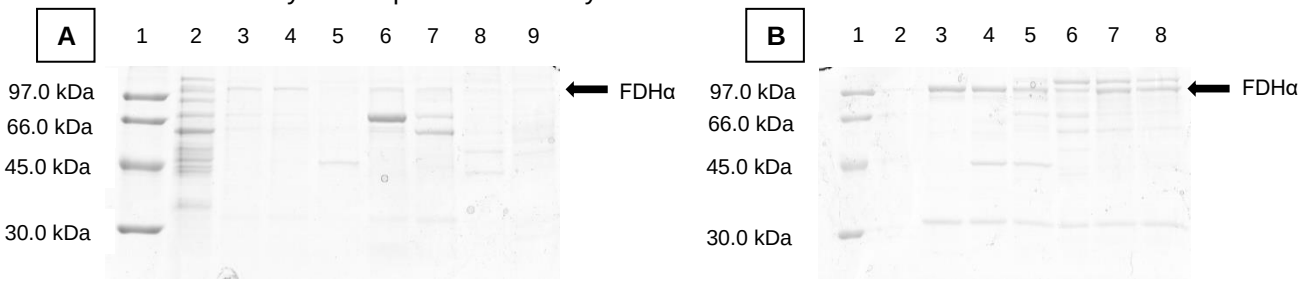

Figure 4: SDS-polyacrylamide gel (12%) to analyse the fractions eluted from the second step of aerobic purification of Elution A **(A)** and Elution B **(B)** of FdhA. In **(A) and (B)**: Lane 1: Amersham Low Molecular Weight Calibration Kit for SDS Electrophoresis (97.0 kDa, 66.0 kDa, 45.0 kDa, 30.0 kDa) (5 µg). In **(A)**: Lane 2: Fraction 0 (8.42 µg); Lane 3: Fraction 1 (5 µg); Lane 4: Fraction 2 (4.22 µg); Lane 5: Fraction 3 (2.01 µg); Lane 6: Fraction 4 (7.24 µg); Lane 7: Fraction 5 (4.97 µg); Lane 8: Fraction 6 (10.04 µg); Lane 9: Fraction 7 (0.66 µg). In **(B)**: Lane 2: Fraction 0 (1.25 µg); Lane 3: Fraction 1 (5 µg); Lane 4: Fraction 2 (5 µg); Lane 5: Fraction 3 (5 µg); Lane 6: Fraction 4 (5 µg); Lane 7: Fraction 5 (5 µg); Lane 8: Fraction 6 (5 µg).

To further evaluate protein stability, the samples used in the CD analysis were recovered and concentrated to perform a Thermal Shift Assay (Table 2).

Table 2: Thermal shift assay of FdhAB and FdhA, with the melting temperate (T_M, temperate at which 50% of the protein is denaturated).

Sample	T_M (ºC)
FdhAB	78.9 ± 0.1
FdhA	66.3 ± 1.0

The melting temperature (T_M) of FdhAB (78.9 ± 0.1 ºC) was significantly higher than the one of FdhA (66.3 ± 1.0 ºC), further supporting the presence of important structural differences between the two proteins.

The kinetic parameters from FdhA were evaluated with the purer sample from the purification of Elution B (P2). FdhAB was also analysed for comparison (Table 3).

Table 3: Kinetic characterization of FdhAB and the FdhA variant. For formate oxidation and CO_2 reduction, catalytic constant (k_{cat} (s^{-1})) and specific activity (U/mg) are represented.

Sample	Formate Oxidation		CO_2 Reduction	
	k_{cat} (s^{-1})	Specific Activity (U/mg)	k_{cat} (s^{-1})	Specific Activity (U/mg)
FdhAB	961 ± 84	417 ± 36	234 ± 13	102 ± 6
FdhA	5.28 ± 0.55	2.86 ± 0.30	1.34 ± 0.08	0.73 ± 0.04

Formate oxidation and CO_2 reduction activity were significantly decreased in FdhA versus FdhAB. It is worth noting that to obtain full activity, a higher concentration of DTT (500 mM) was required to activate the protein in comparison with the regular concentration used (50 mM), possibly due to the longer period of oxygen exposure associated with the additional purification step. Nonetheless, this does not explain the 182-fold decrease in formate oxidation activity and 174-fold decrease in CO_2 reduction activity.

In summary, all these results show that it is possible to obtain the simplified version of the protein, only possessing the α-subunit, but with a significant decrease in expression and activity. These observations, combined with the results obtained from CD spectroscopy indicate that the isolated FdhA variant might have a stability problem, related to unfolded or misfolded regions of the protein. This suggests that the β-subunit can have an important structural and functional role besides electron transfer. The difficulties associated with obtaining enough protein in a pure sample hampered any further additional experimental tests that could be performed to get a more concrete notion of the problem.

Photocatalytic Reduction of CO_2 with FdhAB

One of the most promising applications for FDHs is photocatalysis, with the use of an endless resource, light, to supply energy for catalysis. Furthermore, to gain more insight into relevant mutations that could drive the performance of a photocatalytic system, an easy and commercial photocatalytic setup was created and tested. A system coupling TiO_2 with FdhAB, using a solar simulator, and a system with TiO_2 sensitization with EY, using a LED system emitting at 470 nm, was tested with two different SEDs, cysteine (Cys) and triethanolamine (TEOA).

Table 4: Formate production (mM) at several timepoints for the system with TEOA or Cys coupled to TiO_2 and FdhAB in the Solar Simulator or coupled to Eosin Y, TiO_2 and FdhAB in LEDs.

	Formate Production (mM)			
	SED|TiO_2|FdhAB		SED|Eosin Y|TiO_2|FdhAB	
	TEOA	CYS	TEOA	CYS
1.5 h	2.1 ± 0.1	0.3 ± 0.0	-	-
3 h	3.9 ± 0.1	0.5 ± 0.1	0.3 ± 0.0	0.1 ± 0.0
6 h	-	-	0.4 ± 0.1	0.2 ± 0.0
24 h	-	-	0.9 ± 0.0	0.5 ± 0.1

It is quite noticeable that TEOA significantly outperformed Cys, with higher formate production in both systems (Table 4), with a 2-fold increase and a 7-fold increase with TEOA versus Cys in the system using LEDs and in the system using the Solar Simulator, respectively. These results show that TEOA regenerates EY and TiO_2 more efficiently than Cys. For that, TEOA was selected as the SED for both systems, and their optimization was further pursued.

Firstly, TiO_2 concentration was optimized (varied from 0.44 to 2.175 mg/mL, Figure 5) since the enzyme and TiO_2 interact strongly, therefore the ratio between nanoparticles and enzyme could influence the efficiency of the system.

The two systems reacted differently to variations in TiO_2 concentration, with the sensitized system not showing significant changes in formate production, while in the system without sensitization there was a clear benefit. The increment in TiO_2 linearly increased formate production up to 5.4 mM (3 h), utilizing 1.74 mg/mL of TiO_2, while further increase dropped formate production.

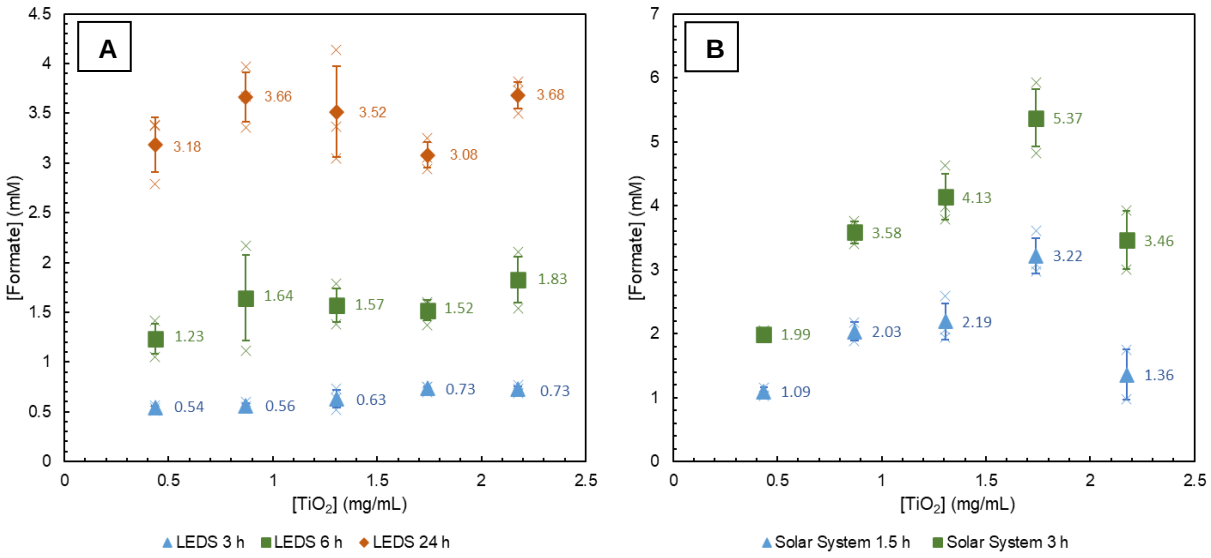

Figure 5: Formate production as a function of TiO_2 concentration used for the system with sensitization using LEDs **(A)** and without sensitization using the Solar Simulator **(B)**. Crosses represent replicates and the error bars the standard deviation.

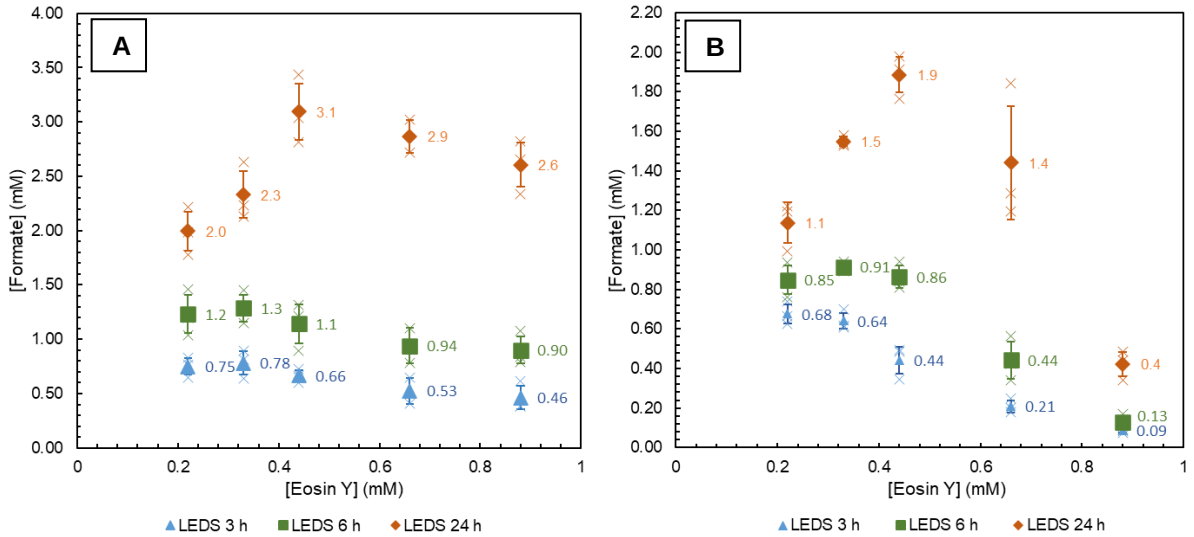

Figure 6: Formate production as a function of Eosin Y concentration used for the system with TEOA|Eosin Y|TiO2 nanoparticles|FdhAB **(A)** and for the system with TEOA|Eosin Y|FdhAB **(B)**, both using LEDS. Crosses represent replicates and the error bars the standard deviation.

Similarly, to evaluate the effect of using different concentrations of EY, this component was varied from 0.22 to 0.88 mM while maintaining the original concentration of TiO_2 used (0.87 mg/mL) (Figure 6A). Furthermore, to analyse if the dye could directly supply electrons to FdhAB, a system without TiO_2 was tested as well (Figure 6B). Interestingly, EY can deliver electrons directly to FdhAB, in a completely metal-free system. However, when comparing both systems, in all concentrations, the TiO_2-sensitized system outperformed the TiO_2-free system. Nonetheless, at 24 h, 0.44 mM of EY outperformed the remaining concentrations studied for both systems, being the chosen concentration.

To validate the three systems in the study, several controls were performed using the optimized concentrations. In the EY systems, with and without TiO_2 nanoparticles, controls without light, without TEOA or without FdhAB were tested and no formate production was obtained, proving that the system only works with the presence of all the components (data not shown). In the case of the systems using only TiO_2, the same controls (no SED, no enzyme or in the dark) were performed as well, besides a control without TiO_2 nanoparticles. Formate production was identified in the control without TEOA and in the control without FdhAB (1.83 ± 0.24 and 0.23 ± 0.01 mM of formate being produced after 3 h, respectively). In the control without TEOA, this can be explained by the presence of DTT which can also act as a SED[35]. In the control without FdhAB, formate production was low and can be residual non-specific TiO_2 catalysis[49].

Overall, the TEOA|TiO_2|FdhAB system in the Solar Simulator outperforms the remaining two systems, resulting in the production of 3.2 ± 0.3 mM of formate with an enzyme turnover of 50 ± 4 s^{-1} after 1.5 h and 5.4 ± 0.5 mM with a turnover of 42 ± 4 s^{-1} after 3 h. However, it is important to note that in this system the use of UV-light and high intensity is demanded. In the case of the systems with sensitization of TiO_2 using the LEDs a formate production of 0.6 ± 0.1 mM with an enzyme turnover of 5.1 ± 0.4 s^{-1} and of 3.1 ± 0.3 mM with a turnover of 3.0 ± 0.2 s^{-1} is attained after 3 and 24 h, respectively. Nonetheless, the single wavelength of 470 nm and a light intensity of 7 W/m^2 is used, therefore when considering system performance and light requirements this system can be advantageous. Furthermore, this system is even effective in a metal-free setup, although with lower production rates.

Computational Optimization of FdhA and FdhAB

FdhA, the simplified version of the protein appears to have stability issues. For this reason, the stabilization of the full α-subunit was studied using the PROSS algorithm[37]. Furthermore, natural proteins are only marginally stable[38], so it would be of high relevance to make FdhAB even more robust and stable, making it more tolerant to mutations in the active site, which could be further explored in order to improve activity. For this reason, an unpublished x-ray structure of FdhAB will be used. For the stabilization of FdhA, the β-subunit with its three iron-sulphur clusters were removed from the structure, whilst for FdhAB stabilization, the full structure was used. For each subunit, a PSSM was generated. To avoid loss of activity, residues at 4 Å the tungsten metal center, the MGDs binding site, the metal sulphide ligand and the iron-sulphur clusters were restricted and fixed. For each optimization, 8 different designs were obtained with different energetic thresholds (from the less permissive design 1 to the more permissive design 8).

As expected, when applying a more permissive energy threshold, the number of mutations that the algorithm incorporates in the design increases (Table 5). When comparing both sets of designs, it is noteworthy that the number of mutations added in FdhAB is higher than the number of mutations added in FdhA for a given threshold, which is curious since FdhAB is a bigger protein, therefore one would expect a higher number of mutations. On the other hand, FdhAB is more stable, since the β-subunit somehow already stabilizes the large subunit. Surprisingly, in FdhAB no mutations were added to the β-subunit in all designs, even in the most permissive

Table 5: FdhA and FdhAB with their respective designs obtained using PROSS. The differences in the number of hydrogen bonds and salt-bridges, mutations to proline, to negatively charged (D/E) or positively charged (K/R) residues are represented. Positive values represent more interactions in the designed proteins and negative values representing fewer interactions, versus the FdhAB or FdhA.

Protein	Total Amino Acids	Mutations	Mutations in Core	Energy (kcal.mol^{-1})	H Bonds	Salt Bridges	X <-> Pro	Negatively Charged	Positively Charged	Isoelectric Point (pI)
FdhA	970	-	-	-2950	-	-	-	-	-	8.61
dFdhA1		124 (13%)	42 (34%)	-3195	12	-11	3	0	1	8.65
dFdhA2		131 (14%)	42 (32%)	-3179	16	-6	3	-1	2	8.74
dFdhA3		147 (15%)	49 (33%)	-3204	11	-8	4	1	3	8.70
dFdhA4		153 (16%)	51 (33%)	-3210	15	7	4	4	8	8.73
dFdhA5		156 (16%)	48 (31%)	-3208	19	-5	3	4	6	8.61
dFdhA6		163 (17%)	50 (31%)	-3226	7	0	4	6	8	8.65
dFdhA7		174 (18%)	56 (32%)	-3237	9	+8	4	3	10	8.84
dFdhA8		200 (21%)	62 (31%)	-3233	1	-6	4	8	6	8.42
FdhAB	1184	-	-	-3618	-	-	-	-	-	8.36
dFdhAB1		90 (8%)	22 (24%)	-3857	10	21	-4	10	6	8.05
dFdhAB2		93 (8%)	22 (24%)	-3852	10	20	-4	9	4	7.95
dFdhAB3		100 (8%)	26 (26%)	-3867	3	29	-4	11	5	7.83
dFdhAB4		105 (9%)	27 (26%)	-3871	4	22	-3	11	6	7.95
dFdhAB5		119 (10%)	31 (26%)	-3875	7	29	-2	11	7	8.03
dFdhAB6		127 (11%)	37 (29%)	-3877	5	28	0	11	8	8.11
dFdhAB7		143 (12%)	42 (29%)	-3892	12	18	1	9	9	8.30
dFdhAB8		172 (15%)	53 (31%)	-3888	7	12	0	11	6	7.93

one (dFdhAB8). Even though FdhAB was optimized one subunit at a time, since the algorithm recognizes the presence of the other subunit, the β-subunit clearly influences the design that PROSS conducts in the α-subunit.

For all designs, there is a decrease in energy in comparison to the original sequence, meaning that the designs are more stable. The profile is similar for the designs of both proteins, with the energy decreasing with the increase in the threshold permissiveness. In the case of design 8, since the algorithm allows the incorporation of mutations with a positive ΔΔG, there is a slight increase in energy. Nonetheless, in both cases design 7 is the one that has a lower energy, with an increase of around 10% in dFdhA7 in comparison to FdhA (-3237 kcal.mol^{-1} and -2950 kcal.mol^{-1}, respectively) and 8% in dFdhAB7 in comparison with FdhAB (-3892 kcal.mol^{-1} and 3618 kcal.mol^{-1}, respectively).

Interestingly, in FdhA each design optimizes different types of interactions. While for the more conservative thresholds (from 1 to 5) the algorithm focuses on increasing H-bonds, for the more permissive designs, it focuses more on electrostatic interactions, with mutations to negatively charged or positively charged amino acids (from design 4 to 8). In FdhAB design the algorithm increases in all models the number of salt-bridges, from 12 to 29 versus FdhAB. There is also a great increase in negatively charged and positively charged amino acids. Furthermore, in the most conservative designs (from dFdhAB1 to dFdhAB5) there is a decrease in prolines, which should contribute to improve the flexibility in certain regions of the protein.

Noteworthy, the presence of the β-subunit alters the energy of the protein, therefore it changes the designs, with more focus being given to salt-bridges and charged amino acids. When comparing the two best designs in terms of energy, dFdhA7 and dFdhAB7, all types of interactions analysed seem to be optimized, possibly explaining why overall these designs seem to have the lower energy, being the most stable. From the 8 designs obtained for each protein, some of them need to be selected for experimental validation.

4. DISCUSSION

As humanity walks towards the future our consciousness of the impact of CO_2 emissions and the need to develop cleaner alternatives to power our society is rising. FDHs are one of the most efficient ways of performing the two electron-reduction of CO_2 to formate, which can tackle both problems. In this work, the generation of a simplified version comprising only the α-subunit was successfully done, however with decreases of turnover of around 200-fold for both formate oxidation and CO_2 reduction in comparison to FdhAB (able to catalyse the reaction with a turnover of 961 ± 84 s^{-1} and of 234 ± 13 s^{-1}, respectively, similar to the ones previously reported of 1310 ± 50 s^{-1} and 315 ± 28 s^{-1}, respectively)[18]. The results obtained for FdhA are similar to the ones obtained with the [NiFe] hydrogenase from *Ralstonia eutropha*. This hydrogenase has a catalytic subunit and an electron transfer subunit in a similar configuration as FdhAB, with the authors removing the small subunit, leading to a 200-fold decrease in H/D exchange activity comparing to the wild-type enzyme[34]. In our case, the abrupt decrease in activity is accompanied by protein expression being impaired (seen by Western-blot and SDS-PAGE), something that in the [NiFe] hydrogenase was not reported.

The reduced protein expression in combination with the results from CD and from the thermal shift assay indicate a protein stability problem. Little is known about the maturation process of FDHs. In the case of FdhAB, it is known that the α-subunit interacts with the β-subunit in the cytoplasm, since only the α-subunit has the signal peptide required for the protein to be translocated to the periplasm. This signal peptide contains a twin-arginine

translocation signal (for the twin-arginine translocation pathway – TAT pathway)[50,51]. Furthermore, the TAT pathway exports fully folded proteins from the cytoplasm to the periplasm, having a folding quality control intrinsic to the process[50,52]. It is known that the maturation of the FDH from *R. capsulatus* occurs through a concerted process, where first subunit assembly occurs and only after, the cofactors and the iron-sulphur clusters are inserted through the help of chaperones, followed by a final folding step after insertion[53,54]. With this in mind, the low expression observed in this work can be explained by two main hypotheses: (i) the β-subunit could be required for α-stabilization and without the presence of the β-subunit proper folding is not acquired and the protein is not translocated to the periplasm due to problems with the folding quality control mechanism and is marked for degradation, explaining the low yields or (ii) proper insertion of the cofactors might be required prior to the formation of the dimer due to the need of having a "pre-folded" protein that has the cofactor binding pocket, which would explain the low activity seen. This work shows the importance of the β-subunit, which in the case of FdhAB appears to be of structural relevance for proper folding of the catalytic subunit and efficient catalysis, with its absence leading to lower yields of protein.

Photocatalysis aims to utilize the endless resource that is light as a source of energy to drive catalytic reactions, being of high potential for the area of sustainability. Several studies have already been performed using FDHs for CO_2 reduction powered by light, including with FdhAB[35]. Due to the unfortunate loss of activity in FdhA, the photocatalytic approach was only explored using FdhAB. For this, a system using TEOA|TiO_2|FdhAB was developed with high formate productions (3.2 ± 0.3 mM) and high turnover (50 ± 4 s^{-1}) being obtained after 1.5 h. As previously reported, TiO_2 interacts strongly with FdhAB, with more than 60% of FdhAB remaining absorbed to the nanoparticle even after washing with 3 M of KCl, possibly due to the interaction between TiO_2 and negatively charged amino acids at the surface of FdhAB[35]. However, this system is only able to absorb UV radiation, with the results being obtained under supply of high-intensity light (7000 W/m^2 from 320-450 nm). Therefore, we successfully sensitized TiO_2 with EY obtaining 0.6 ± 0.1 mM of formate with a turnover of 5.1 ± 0.4 s^{-1} with the energy used being supplied at a single wavelength in the visible region, 470 nm, and in a much lower intensity (7 W/m^2), making the process more energetically efficient. Furthermore, in comparison to the previously described system with TEOA|DPP|TiO_2|FdhAB where a turnover of 5 ± 0.6 s^{-1} with 100 W/m^2 light-intensity above 420 nm was used[35], a similar turnover was obtained using EY, which is commercially available and with less input of energy. Even further, EY is also able to form multilayer structures by complexation with metal ions, which already has been performed for H_2 evolution with 3-fold increase in production[55], meaning that this system can be further improved. EY was even able to transfer electrons directly to FdhAB in a metal-free version of the system even though at lower rates, showing the versatility of EY.

With the removal of the β-subunit causing abrupt effects in the stability of the α-subunit the stabilization of the full α-subunit was attempted using PROSS algorithm[37]. It is especially applicable to alleviating problems of low expression levels and misfolding. Furthermore, it has shown wide success in several studies using different types of proteins[37,56,57]. In parallel, the protocol was also employed to FdhAB since natural proteins often suffer from marginal stability[38]. For each protein, 8 optimized models were obtained, with a high number of mutations being added even in the stricter thresholds. In FdhAB, fewer mutations were added in comparison with FdhA, which was unexpected since even though FdhAB is more stable, since it is a larger protein one would expect that more mutations would be added, especially in the more permissive threshold. The lack of mutations in the β-subunit, possibly due to large restrictions being applied near the three iron-sulphur clusters, coupled to the change in the environment of the α-subunit due to the presence of the β-subunit, led to a significant change in the number of mutations for a given threshold. Even though the creators of PROSS suggest that model 7 is in most cases the ideal one, due to the low risk of false positives[37], the high number of mutations being incorporated in the design variants with this threshold adds some uncertainty regarding the final outcome. In FdhA, the protein is suspected to be unstable, therefore it is expected that a higher number of alterations are required for stabilization. In FdhAB, we are dealing with a protein that is shown to be operationally stable, with a high T_M as seen in this study and previously reported[18]. Nonetheless, being able to increase the yields of protein and increase stability to implement a functional design protocol for improved activity[58] would be highly beneficial. With this in mind, along with the models dFdhA7 and dFdhAB7 it would be of great interest to test two additional models to reduce the risk of the high number of mutations proposed in these models. It is hard to predict how each model will behave experimentally, however, PROSS has been proven to work, even in far worse settings than this one[56,57].

5. ACKNOWLEDGEMENTS

This document was written and made publically available as an institutional academic requirement and as a part of the evaluation of the MSc thesis in Biotecnology of the author at Instituto Superior Técnico. The work described herein was performed at the Bacterial Energy Metabolism group of Instituto de Tecnologia Química e Biológica António Xavier (ITQB), during the period of September 2020 to July 2021, under the supervision of Dr. Inês Cardoso Pereira and Dr. Arsénio do Carmo Sales Mendes Fialho.

6. REFERENCES

1. Dupuis, M. *et al.* Frontiers, Opportunities, and Challenges in Biochemical and Chemical Catalysis of

CO_2 Fixation. *Chem. Rev.* **113**, 6621–6658 (2013).
2. Maia, L. B., Moura, I. & Moura, J. J. G. Molybdenum and tungsten-containing formate dehydrogenases: Aiming to inspire a catalyst for carbon dioxide utilization. *Inorganica Chim. Acta* **455**, 350–363 (2017).
3. Masson-Delmotte, V., P. Zhai, H.-O. Pörtner, D. Roberts, J. Skea, P. R. S., A. Pirani, W. Moufouma-Okia, C. Péan, R. Pidcock, S. Connors, J.B.R. Matthews, Y. Chen, X. Zhou, M. I. G. & E. Lonnoy, T. Maycock, M. Tignor, and T. W. *Global Warming of 1.5°C. An IPCC Special Report on the impacts of global warming of 1.5°C above pre-industrial levels and related global greenhouse gas emission pathways, in the context of strengthening the global response to the threat of climate change,. Summary for PolicyMakers In: Global Warming of 1,5 °C* (2018).
4. United Nations. *Emissions Gap Report 2019*. *Emissions Gap Report 2019* (2019).
5. Sekera, J. & Lichtenberger, A. Assessing Carbon Capture: Public Policy, Science, and Societal Need. *Biophys. Econ. Sustain.* **5**, 1–28 (2020).
6. Sanz-Pérez, E. S., Murdock, C. R., Didas, S. A. & Jones, C. W. Direct Capture of CO_2 from Ambient Air. *Chem. Rev.* **116**, 11840–11876 (2016).
7. Munshi, P., Main, A. D., Linehan, J. C., Tai, C. C. & Jessop, P. G. Hydrogenation of carbon dioxide catalyzed by ruthenium trimethylphosphine complexes: The accelerating effect of certain alcohols and amines. *J. Am. Chem. Soc.* **124**, 7963–7971 (2002).
8. Tanaka, R., Yamashita, M., Chung, L. W., Morokuma, K. & Nozaki, K. Mechanistic studies on the reversible hydrogenation of carbon dioxide catalyzed by an Ir-PNP complex. *Organometallics* **30**, 6742–6750 (2011).
9. Hull, J. F. *et al.* Reversible hydrogen storage using CO_2 and a proton-switchable iridium catalyst in aqueous media under mild temperatures and pressures. *Nat. Chem.* **4**, 383–388 (2012).
10. Filonenko, G. A., Van Putten, R., Schulpen, E. N., Hensen, E. J. M. & Pidko, E. A. Highly efficient reversible hydrogenation of carbon dioxide to formates using a ruthenium PNP-pincer catalyst. *ChemCatChem* **6**, 1526–1530 (2014).
11. Shi, J. *et al.* Enzymatic conversion of carbon dioxide. *Chem. Soc. Rev.* **44**, 5981–6000 (2015).
12. Alissandratos, A. & Easton, C. J. Biocatalysis for the application of CO_2 as a chemical feedstock. *Beilstein J. Org. Chem.* **11**, 2370–2387 (2015).
13. Enthaler, S., Von Langermann, J. & Schmidt, T. Carbon dioxide and formic acid - The couple for environmental-friendly hydrogen storage? *Energy Environ. Sci.* **3**, 1207–1217 (2010).
14. Wang, W.-H., Feng, X. & Bao, M. *Transformation of CO_2 to Formic Acid or Formate Over Heterogeneous Catalysts*. (2018).
15. Choe, H. *et al.* Efficient CO_2-reducing activity of NAD-dependent formate dehydrogenase from Thiobacillus sp. KNK65MA for formate production from CO_2 gas. *PLoS One* **9**, 14–16 (2014).
16. De Bok, F. A. M. *et al.* Two W-containing formate dehydrogenases (CO_2-reductases) involved in syntrophic propionate oxidation by Syntrophobacter fumaroxidans. *Eur. J. Biochem.* **270**, 2476–2485 (2003).
17. Reda, T., Plugge, C. M., Abram, N. J. & Hirst, J. Reversible interconversion of carbon dioxide and formate by an electroactive enzyme. *Proc. Natl. Acad. Sci. U. S. A.* **105**, 10654–10658 (2008).
18. Oliveira, A. R. *et al.* Toward the Mechanistic Understanding of Enzymatic CO_2 Reduction. *ACS Catal.* **10**, 3844–3856 (2020).
19. Maia, L. B., Fonseca, L., Moura, I. & Moura, J. J. G. Reduction of Carbon Dioxide by a Molybdenum-Containing Formate Dehydrogenase: A Kinetic and Mechanistic Study. *J. Am. Chem. Soc.* **138**, 8834–8846 (2016).
20. Schuchmann, K. & Müller, V. Direct and reversible hydrogenation of CO_2 to formate by a bacterial carbon dioxide reductase. *Science (80).* **342**, 1382–1385 (2013).
21. Schwarz, F. M., Schuchmann, K. & Müller, V. Hydrogenation of CO_2 at ambient pressure catalyzed by a highly active thermostable biocatalyst. *Biotechnol. Biofuels* **11**, 1–11 (2018).
22. Gonzalez, P. J. *et al.* Periplasmic nitrate reductases and formate dehydrogenases: Biological control of the chemical properties of Mo and W for fine tuning of reactivity, substrate specificity and metabolic role. *Coord. Chem. Rev.* **257**, 315–331 (2013).
23. Raaijmakers, H. C. A. & Romão, M. J. Formate-reduced *E. coli* formate dehydrogenase H: The reinterpretation of the crystal structure suggests a new reaction mechanism. *J. Biol. Inorg. Chem.* **11**, 849–854 (2006).
24. Jormakka, M., Törnroth, S., Byrne, B. & Iwata, S. Molecular basis of proton motive force generation: Structure of formate dehydrogenase-N. *Science (80).* **295**, 1863–1868 (2002).
25. Raaijmakers, H. *et al.* Gene sequence and the 1.8 Å crystal structure of the tungsten-containing formate dehydrogenase from *Desulfovibrio gigas*. *Structure* **10**, 1261–1272 (2002).
26. Mota, C. S. *et al.* The mechanism of formate oxidation by metal-dependent formate dehydrogenases. *J. Biol. Inorg. Chem.* **16**, 1255–1268 (2011).
27. Cerqueira, N. M. F. S. A., Fernandes, P. A., Gonzalez, P. J., Moura, J. J. G. & Ramos, M. J. The sulfur shift: An activation mechanism for periplasmic nitrate reductase and formate dehydrogenase. *Inorg. Chem.* **52**, 10766–10772 (2013).
28. Tiberti, M., Papaleo, E., Russo, N., De Gioia, L. & Zampella, G. Evidence for the formation of a Mo-H intermediate in the catalytic cycle of formate dehydrogenase. *Inorg. Chem.* **51**, 8331–8339 (2012).
29. Dong, G. & Ryde, U. Reaction mechanism of formate dehydrogenase studied by computational methods. *J. Biol. Inorg. Chem.* **23**, 1243–1254 (2018).
30. Lee, S. H., Choi, D. S., Kuk, S. K. & Park, C. B. Photobiocatalysis: Activating Redox Enzymes by Direct or Indirect Transfer of Photoinduced Electrons. *Angew. Chemie - Int. Ed.* **57**, 7958–7985 (2018).
31. Corma, A. & Garcia, H. Photocatalytic reduction of CO_2 for fuel production: Possibilities and challenges. *J. Catal.* **308**, 168–175 (2013).
32. Ameta, R., Solanki, M. S., Benjamin, S. & Ameta, S. C. Photocatalysis. in *Advanced Oxidation Processes for Wastewater Treatment: Emerging Green Chemical Technology* 135–175 (2018).
33. Pellegrin, Y. & Odobel, F. Sacrificial electron donor reagents for solar fuel production. *Comptes Rendus Chim.* (2016).
34. Caserta, G. *et al.* The large subunit of the regulatory [NiFe] hydrogenase fromRalstonia eutropha- a minimal hydrogenase? *Chem. Sci.* **11**, 5453–5465 (2020).
35. Miller, M. *et al.* Interfacing Formate Dehydrogenase with Metal Oxides for the Reversible Electrocatalysis and Solar-Driven Reduction of Carbon Dioxide. *Angew. Chemie - Int. Ed.* **58**, 4601–4605 (2019).
36. Chowdhury, P., Gomaa, H. & Ray, A. K. Sacrificial hydrogen generation from aqueous triethanolamine with Eosin Y-sensitized Pt/TiO_2 photocatalyst in UV, visible and solar light irradiation. *Chemosphere* **121**, 54–61 (2015).
37. Goldenzweig, A. *et al.* Automated Structure- and Sequence-Based Design of Proteins for High Bacterial Expression and Stability. *Mol. Cell* **63**, 337–346 (2016).
38. Goldenzweig, A. & Fleishman, S. J. Principles of Protein Stability and Their Application in Computational Design. *Annu. Rev. Biochem.* **87**, 105–129 (2018).

39. Keller, K. L., Wall, J. D. & Chhabra, S. *Methods for Engineering Sulfate Reducing Bacteria of the Genus Desulfovibrio*. *Synthetic Biology, Part A* vol. 497 (Elsevier Inc., 2011).
40. Micsonai, A. *et al.* Accurate secondary structure prediction and fold recognition for circular dichroism spectroscopy. *Proc. Natl. Acad. Sci. U. S. A.* **112**, E3095–E3103 (2015).
41. Micsonai, A. *et al.* BeStSel: A web server for accurate protein secondary structure prediction and fold recognition from the circular dichroism spectra. *Nucleic Acids Res.* **46**, W315–W322 (2018).
42. Alford, R. F. *et al.* The Rosetta all-atom energy function for macromolecular modeling and design. *J. Chem. Theory Comput* **13**, 3031–3048 (2017).
43. Hanwell, M. D., Curtis, D. E., Lonie, D. C. & Vandermeersch, T. Avogadro: an advanced semantic chemical editor, visualization, and analysis platform. *J. Cheminform.* **4**, (2012).
44. Altschul, S. F., Gertz, E. M., Agarwala, R., Schäffer, A. A. & Yu, Y. K. PSI-BLAST pseudocounts and the minimum description length principle. *Nucleic Acids Res.* **37**, 815–824 (2009).
45. Li, W. & Godzik, A. Cd-hit: A fast program for clustering and comparing large sets of protein or nucleotide sequences. *Bioinformatics* **22**, 1658–1659 (2006).
46. Humphrey, W., Dalke, A. & Schulten, K. VMD: Visual Molecular Dynamics. *J. Mol. Graph.* **14**, 33–98 (1996).
47. O'Meara, M. J. *et al.* Combined covalent-electrostatic model of hydrogen bonding improves structure prediction with Rosetta. *J. Chem. Theory Comput.* **11**, 609–622 (2015).
48. Gasteiger, E. *et al.* ExPASy: The proteomics server for in-depth protein knowledge and analysis. *Nucleic Acids Res.* **31**, 3784–3788 (2003).
49. Habisreutinger, S. N., Schmidt-Mende, L. & Stolarczyk, J. K. Photocatalytic reduction of CO_2 on TiO_2 and other semiconductors. *Angew. Chemie - Int. Ed.* **52**, 7372–7408 (2013).
50. Palmer, T. & Berks, B. C. The twin-arginine translocation (Tat) protein export pathway. *Nat. Rev. Microbiol.* **10**, 483–496 (2012).
51. Jormakka, M., Byrne, B. & Iwata, S. Formate dehydrogenase - A versatile enzyme in changing environments. *Curr. Opin. Struct. Biol.* **13**, 418–423 (2003).
52. DeLisat, M. P., Tullman, D. & Georgiou, G. Folding quality control in the export of proteins by the bacterial twin-arginine translocation pathway. *Proc. Natl. Acad. Sci. U. S. A.* **100**, 6115–6120 (2003).
53. Hartmann, T., Schwanhold, N. & Leimkühler, S. Assembly and catalysis of molybdenum or tungsten-containing formate dehydrogenases from bacteria. *Biochim. Biophys. Acta - Proteins Proteomics* **1854**, 1090–1100 (2015).
54. Schwanhold, N., Iobbi-Nivol, C., Lehmann, A. & Leimkühler, S. Same but different: Comparison of two system-specific molecular chaperones for the maturation of formate dehydrogenases. *PLoS One* **13**, 1–24 (2018).
55. Li, Y., Guo, M., Peng, S., Lu, G. & Li, S. Formation of multilayer-Eosin Y-sensitized TiO_2 via Fe^{3+} coupling for efficient visible-light photocatalytic hydrogen evolution. *Int. J. Hydrogen Energy* **34**, 5629–5636 (2009).
56. Campeotto, I. *et al.* One-step design of a stable variant of the malaria invasion protein RH5 for use as a vaccine immunogen. *Proc. Natl. Acad. Sci. U. S. A.* **114**, 998–1002 (2017).
57. Zahradník, J. *et al.* Flexible regions govern promiscuous binding of IL-24 to receptors IL-20R1 and IL-22R1. *FEBS J.* **286**, 3858–3873 (2019).
58. Khersonsky, O. *et al.* Automated Design of Efficient and Functionally Diverse Enzyme Repertoires. *Mol. Cell* **72**, 178–186 (2018).